Hindawi
Complexity
Volume 2024, Article ID 9832810, 1 page
https://doi.org/10.1155/2024/9832810

WILEY | Hindawi

Retraction

Retracted: Application of Compound Control Method Based on WOA in Micropositioning Stage of SICM

Complexity

Received 23 January 2024; Accepted 23 January 2024; Published 24 January 2024

This article has been retracted by Hindawi following an investigation undertaken by the publisher [1]. This investigation has uncovered evidence of one or more of the following indicators of systematic manipulation of the publication process:

(1) Discrepancies in scope

(2) Discrepancies in the description of the research reported

(3) Discrepancies between the availability of data and the research described

(4) Inappropriate citations

(5) Incoherent, meaningless and/or irrelevant content included in the article

(6) Manipulated or compromised peer review

The presence of these indicators undermines our confidence in the integrity of the article's content and we cannot, therefore, vouch for its reliability. Please note that this notice is intended solely to alert readers that the content of this article is unreliable. We have not investigated whether authors were aware of or involved in the systematic manipulation of the publication process.

Wiley and Hindawi regrets that the usual quality checks did not identify these issues before publication and have since put additional measures in place to safeguard research integrity.

We wish to credit our own Research Integrity and Research Publishing teams and anonymous and named external researchers and research integrity experts for contributing to this investigation.

The corresponding author, as the representative of all authors, has been given the opportunity to register their agreement or disagreement to this retraction. We have kept a record of any response received.

References

[1] H. Wen, X. Lu, S. Zhao, X. Liu, Y. Yang, and S. Leng, "Application of Compound Control Method Based on WOA in Micropositioning Stage of SICM," *Complexity*, vol. 2021, Article ID 5537998, 10 pages, 2021.

Hindawi
Complexity
Volume 2021, Article ID 5537998, 10 pages
https://doi.org/10.1155/2021/5537998

Research Article

Application of Compound Control Method Based on WOA in Micropositioning Stage of SICM

Huiting Wen, Xiaolong Lu, Shiping Zhao, Xiaoyu Liu, Yang Yang, and Song Leng

School of Mechanical Engineering, Sichuan University, Chengdu 610065, Sichuan, China

Correspondence should be addressed to Shiping Zhao; spzhao@scu.edu.cn

Received 5 February 2021; Revised 9 April 2021; Accepted 19 April 2021; Published 30 April 2021

Academic Editor: Zhihan Lv

Positioning accuracy of micropositioning stage in scanning ion conductance microscopy is the key to obtain high-precision scanning model. Most piezoelectric ceramic micromotion platforms are used for that, and hysteresis characteristics are the main reason for the nonlinear characteristics of piezoelectric ceramics and the influence on the control accuracy. In order to solve this problem, backpropagation algorithm based on whale optimization algorithm is used to model the hysteresis, which is directly used as a feedforward controller to compensate the hysteresis effect, and the robust adaptive moving average control method is used for feedback control. The results show that the hysteresis model of backpropagation algorithm based on the whale optimization algorithm can fit the hysteresis curve well, and the maximum fitting error is 0.2050 μm, only 0.256%. By adopting feedforward and feedback, feedforward robust adaptive moving average control algorithm decreases the hysteresis from 17.64% to 2.51%, which enables the output of the piezoelectric ceramic controller to track the expected displacement well and makes it possible to improve the scanning accuracy.

1. Introduction

Scanning ion conductance microscopy (SICM) [1], as a member of the scanning probe microscope (SPM) [2], has been developing for thirty years since 1989 and applied to many areas, such as surface topography measurement [3], nanoscale operation [4], cell volume measurement [5], cell mechanical properties research [6], and cell dynamics research [7]. It has been widely used in life science, medicine, materials science, nanofabrication, and other fields. SICM has edges on in situ noncontact scanning, real-time observation under physiological conditions, and scanning without sample pretreatment, especially on nondestructive testing of soft samples which make it become an important measurement tool for living biological samples in practical applications.

High-precision micro-nanoscale positioning is an important condition for 3D morphology reconstruction by SICM. In order to achieve this goal, nanoscale high-precision control of the piezoelectric ceramic actuator is required [8]. However, the hysteresis of piezoelectric materials results in a nonlinear relationship between the input voltage and output displacement, which seriously affects the positioning accuracy, and leads to the distortion of the scanned image of the samples. Therefore, corresponding compensation measures should be adopted to compensate and control the hysteresis characteristics, so that the output displacement can track the expected displacement well and realize high-precision sample scanning.

At present, there are mainly three methods for compensating the hysteresis of piezoelectric ceramics: charge control method, feedforward open-loop control based on the hysteresis inverse model, and closed-loop control based on feedback [9]. In practical applications, it is difficult to measure the charge directly, and we can choose to integrate the current instead of measuring the charge [10]. But the integration also causes the accumulation of errors, so the charge control method is not suitable for long-term application in the online control of piezoelectric ceramic drivers [11]. In the open-loop control, the inverse models of creep, vibration, and hysteresis are used in series to reduce the nonlinearity of the system. At the same time, the closed-loop

control method based on feedback is widely used in the control field of piezoelectric actuator because it can effectively suppress unknown interference, correct model error, and improve tracking accuracy and other advantages.

All the above three control methods can compensate the error caused by hysteresis nonlinearity. However, the control accuracy and efficiency are not ideal when using a single control method. Wang Xiaodong et al. used the Duhem inverse model and PID as a control method, and the experimental results showed that the maximum fitting error was less than 0.2 μm [12]. Based on linear characteristics, Kuhnen et al. used adaptive law to identify the characteristics of the inverse observer and converted it into controller parameters, thus reducing the maximum linear error of the system by an order of magnitude [13]. Mynderse et al. proposed an inverse model as a feedforward, which did not need to know the expected trajectory in advance, and used linear quadratic regulator (LQR) as a feedback controller, to effectively reduce the compensated error and the hysteresis nonlinearity by 91.5% [14]. Yu Zhiliang et al. linearized the improved PI model for compensation of hysteresis characteristics and proposed a composite control algorithm combining feedforward and incremental PID algorithm. When the inputs are 10 Hz and 100 Hz amplitude-sinusoidal and equal-amplitude-sinusoidal curves, the model error was within 0.59% [15].

Because the feedforward open-loop control method cannot realize the steady state of the piezoelectric ceramic actuator, and feedback control cannot achieve the stability requirements of the system, in this paper, we adopt the combination of feedforward and feedback control, increase the system robustness and adaptive ability, and reduce the impact of uncertainty on the system, to realize the compensation for the characteristics of the piezoelectric hysteresis and accurate control of scanning probe in SICM.

2. Methods and Materials

In this section, for the model identification of piezoelectric ceramic system, the basic principle of backpropagation algorithm based on whale optimization algorithm applied in hysteresis polynomial modeling is introduced. For system control, the principle of moving average control, robust control, and feedforward robust adaptive moving average control (FRAMAC) is explained. The basic equipment and materials used in the experiment are described.

2.1. Backpropagation Algorithm Based on Whale Optimization Algorithm. Because of the hysteresis characteristic of piezoelectric ceramic actuator, the input and output of the system show a many-to-many relationship. In order to model and control, backpropagation algorithm is introduced to improve the original mapping relationship into one-to-one. The whale optimization algorithm is adopted to establish the polynomial model, and then we expand the input space, use the input voltage of the piezoelectric ceramics and the output displacement of polynomial hysteresis model as the input of the BP neural network and the actual output as the output of the BP neural network, and finally set up the hysteresis model of the piezoelectric drive.

2.1.1. Whale Optimization Algorithm. The whale optimization algorithm (WOA) was proposed by an Australian scholar Seyedali Mirjalili, which was inspired by whale foraging behavior, and a new metaheuristic optimization algorithm was proposed in 2016 [16]. WOA simulates the hunting behavior of humpback whales, as shown in Figure 1. When foraging, humpback whales will advance along the spiral path and create unique netted bubbles to surround the prey. This unique hunting behavior gives rise to a new intelligent algorithm to achieve the solution of the objective function [17, 18].

Whale optimization algorithm can be divided into three types of behavior: search for prey, encircle and shrink, and spiral update.

(1) Search for Prey. At this stage, humpback whales search randomly because there is no specific target prey and take the location of another humpback whale as the target location, which expands the search scope and achieves the goal of global search. This behavior is expressed by the following equation:

$$\vec{X}(t+1) = \vec{X}_{\text{rand}}(t) - \vec{A} \cdot \vec{D}, \tag{1}$$

$$\vec{D} = \left| \vec{C} \cdot \vec{X}_{\text{rand}}(t) - \vec{X}(t) \right|, \tag{2}$$

where $\vec{A}$ and $\vec{C}$ are the coefficient vectors and calculated as follows:

$$\vec{A} = 2\vec{a} \cdot \vec{r} - \vec{a}, \tag{3}$$

$$\vec{C} = 2\vec{r}, \tag{4}$$

where $\vec{r}$ represents the random vector in the interval [0,1], t is the number of current iterations, $t_{\max}$ is the maximum number of iterations, $\vec{a}$ is the convergence factor, and its value decreases linearly from 2 to 0:

$$\vec{a} = 2 - \frac{2t}{t_{\max}}. \tag{5}$$

When $|A| > 1$, the humpback whale is in the stage of foraging. If $|A| \le 1$, the humpback whale is in the phase of encircle and shrink or spiral update.

(2) Encircle and Shrink. During the encircle and shrink phase, humpback whales identify the location of their prey and surround it. Since the prey's position is unknown at this time, we assume that the current optimal solution is the target prey, and let it approach the optimal solution. The equation is given by

$$\vec{X}(t+1) = \vec{X^*}(t) - \vec{A} \cdot \vec{D}, \tag{6}$$

$$\vec{D} = \left| \vec{C} \cdot \vec{X^*}(t) - \vec{X}(t) \right|, \tag{7}$$

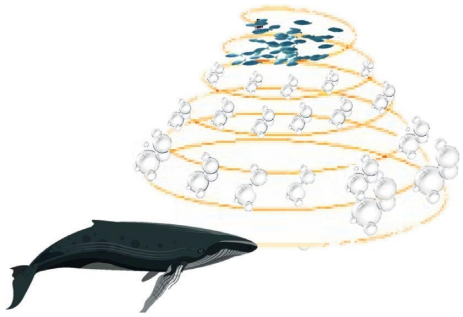

Figure 1: Hunting behavior of humpback whales.

where $\overrightarrow{X^*}(t)$ is the current optimal solution. The humpback whale updates its position according to the current optimal solution $\overrightarrow{X^*}(t)$, and the position around the optimal solution can be obtained by adjusting the value of $\overrightarrow{A}$ and $\overrightarrow{C}$. Formula (7) allows humpback whales to appear anywhere near their prey.

(3) Spiral Update. When hunting prey, humpback whales approach the optimal whale position in a spiral path, calculate the distance between the whale and the prey, and then establish a spiral equation between the positions of the whale and the prey to simulate the spiral motion of humpback whales as shown in the following equation:

$$\begin{aligned}\overrightarrow{X}(t+1) &= \overrightarrow{D}\cdot e^{bl}\cdot \cos(2\pi l) + \overrightarrow{X^*}(t),\\ \overrightarrow{D} &= \left|\overrightarrow{X^*}(t) - \overrightarrow{X}(t)\right|.\end{aligned} \tag{8}$$

where $\overrightarrow{D}$ is the distance between the current position of humpback whale and the optimal solution, b is the constant defining the shape of spiral curve, which is usually 1, and l represents the random vector in the interval [0, 1].

In fact, humpback whales not only follow the spiral path to their prey, but also by means of encircle and shrink. The enclosing contraction behavior is realized by reducing the convergence factor $\overrightarrow{a}$ in equation (5). When it linearly decreases from 2 to 0 with the number of iterations, $\overrightarrow{A}$ is the random value in the interval $[-a, a]$. The two behaviors are simulated at the same time. It is assumed that, during the optimization process, whales chose to surround the contraction path or spiral path with a 50% probability to update the position. The mathematical model is as follows:

$$\overrightarrow{X}(t+1) = \begin{cases} \overrightarrow{X^*}(t) - \overrightarrow{A}\cdot\overrightarrow{D}, & \text{if } p < 0.5,\\ \overrightarrow{D}\cdot e^{bl}\cdot \cos(2\pi l) + \overrightarrow{X^*}(t), & \text{if } p \geq 0.5.\end{cases} \tag{9}$$

The above equation p represents a random number in the interval [0,1]. The latest position of the humpback whale can reach any position between the original position and the current best position.

2.1.2. Backpropagation Algorithm. In 1986, Professor David Runelhart et al. proposed the error backpropagation algorithm (BP algorithm). BP algorithm is generally multilayered, with a hidden layer between the input layer and the output layer. The hidden layer can be one or more layers. The algorithm of error backpropagation is adopted to adjust the weight. The topology mechanism is shown in Figure 2.

When the number of neurons in the input layer is n, in the hidden layer is l, and in the output layer is m.x_1, $x_2 \ldots x_n$ is input signal, g_1, $g_2 \ldots g_m$ is the predicted value, w_{ij} is the connection weight of the input layer to the hidden layer, w_{jk} is the connection weight of the hidden layer to the output layer, and N is the number of iterations; then, the algorithm steps of the BP neural network are as follows:

Step 1: initialize the network, and select the random values between (–1,1) to assign weights w_{ij} and w_{jk} and the threshold values α_j and θ_k.

Step 2: calculate the input of the hidden layer s_j:

$$s_j = \sum_{i=1}^{n} w_{ij}x_i - \alpha_j. \tag{10}$$

Step 3: the transfer function of the hidden layer is $f(x)$ and then the output of the hidden layer b_j is given by

$$b_j = f\left(s_j\right). \tag{11}$$

Step 4: calculate the output layer of the BP neural network g_k:

$$g_k = \sum_{k=1}^{m} w_{jk}b_j - \theta_k. \tag{12}$$

Step 5: according to the output response of the BP neural network with the actual output, the error d_t^k and performance index E of the output layer are as follows:

$$\begin{aligned} d_t^k &= y_k - g_k,\\ E &= \frac{1}{2}\left(d_t^k\right)^2.\end{aligned} \tag{13}$$

Step 6: use δ reverse calculation to calculate the hidden layer error e_{jk}:

$$e_{jk} = \left[\sum_{t=1}^{n} d_t^k w_{jk}\right] * b_j * \left(1 - b_j\right). \tag{14}$$

Step 7: modify the w_{jk} and θ_k:

$$w_{jk}(N+1) = w_{jk}(N) + \beta d_t^k b_j, \tag{15}$$

$$\theta_k(N+1) = \theta_k(N) + \beta d_t^k. \tag{16}$$

Step 8: modify w_{ij} and α_j:

$$w_{ij}(N+1) = w_{ij}(N) + \gamma e_{jk}s_j, \tag{17}$$

$$\alpha_i(N+1) = \alpha_i(N) + \gamma e_{jk}. \tag{18}$$

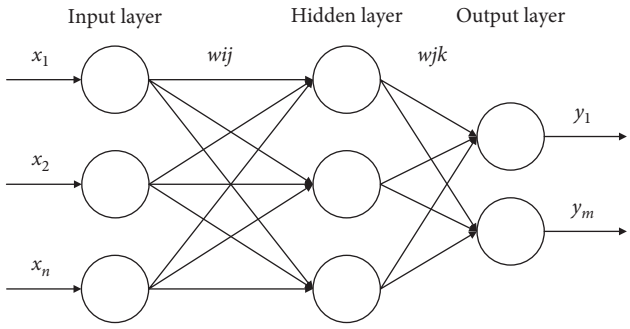

Figure 2: BP neural network.

Step 9: $k \longrightarrow k+1$, return to Step 2 for cyclic calculation until the modeling error is less than the expected error.

Backpropagation algorithm is a local optimal algorithm, and the convergence speed is slow. In order to obtain a more accurate hysteresis model, WOA is used to optimize the BP algorithm to establish a polynomial hysteresis inverse model of piezoelectric ceramic actuator after comparing various improved methods [19–21].

2.1.3. Backpropagation Algorithm Based on Whale Optimization Algorithm. Whale optimization algorithm has the advantages of clear concept, easy implementation, and no need of gradient information. It has been widely used in many fields. Because of its good global searching ability, it is used to model the hysteresis polynomial of the PZT actuator. The flowchart of backpropagation algorithm based on whale algorithm is shown in Figure 3. The algorithm steps are as follows:

Step 1: initialize the parameters, determine the population number N, the maximum number of iterations $t_{\max}$, and the fitness function.

Step 2: calculate the fitness function value of each humpback whale to get the optimal fitness function value and its position vector.

Step 3: calculate and get $\overrightarrow{A}$ and $\overrightarrow{C}$ according to equations (3) and (4).

Step 4: if $|A| > 1$, update the position of the next generation according to equation (1).

Step 5: if $|A| \le 1$, update the position of the next generation according to equation (9).

Step 6: calculate the error of the polynomial hysteresis model. If the optimization standard is met, go to the next step; if not, return to Step 3 for cyclic calculation.

Step 7: initialize the network, and select the random values between (–1,1) to assign the weight values w_{ij} and w_{jk} and the threshold values α_j and θ_k.

Step 8: the forward propagation operation is adopted, and the expected output is obtained according to equation (12), and the error is calculated.

Step 9: the backpropagation operation is adopted, and the network weight and threshold are corrected according to equations (15)~(18).

Step 10: $k \longrightarrow k+1$, return to Step 8 for cyclic calculation until the error is less than the expected error.

2.2. Model Control. Feedforward control, moving average control, adaptive control, and robust control have their own advantages and applicable conditions. The research shows that if a single feedforward is used, the hysteresis characteristics of the system can be linearized to achieve the stability requirements, but not the steady state, so it is necessary to introduce a feedback. In the operation process of the piezoelectric ceramic actuator, the structure or parameters will change to some extent, which requires the use of the self-tuning method, through online identification to obtain parameters to update the control parameters. Because of the influence of external disturbance or uncertainty, such as noise, it is difficult for the system to return to the original equilibrium state. Therefore, by using robust control and adaptive control in the feedback controller, the original algorithm is improved and feedforward robust adaptive moving average control method is formed (FRAMAC), as shown in Figure 4.

In Figure 4, in order to reduce the effect of hysteresis nonlinearity on the output displacement, the hysteresis inverse model is generally used to linearize the hysteresis of piezoelectric ceramics. In this paper, a hysteresis polynomial inverse model with expected displacement as input and control voltage as output is established, and the inverse model is directly used as a feedforward controller to compensate the hysteresis effect of piezoelectric ceramics, thus eliminating the process of calculating the inverse hysteresis model. Then, the linearized hysteresis is controlled by a robust adaptive moving average controller, and a feedforward robust adaptive moving average control based on the inverse model of hysteresis polynomial is established.

2.2.1. Moving Average Control. Controlled autoregressive moving average (CARMA) model is used to describe the mathematical models for controlled processes. Consider the input/output model:

$$A(q)y(k) = B(q)u(k) + C(q)e(k). \tag{19}$$

The moving average method can be adopted when the following four conditions are met:

① $\deg C = \deg A = n$

② $\deg B = m$

③ $A, C$is the first polynomial, where the zero of the polynomial C must be in the unit circle

④ $d_0 = \deg A - \deg B$

In steady state, the steady-state variance of output data is adopted as the control objective function, and the performance index is $J = E\{y^2(k)\}$ where E represents the mathematical expectation acting on the noise system.

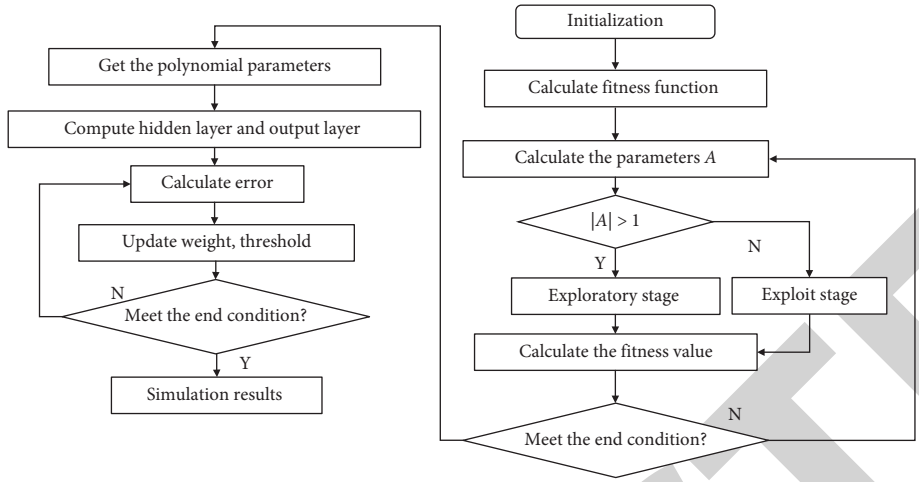

Figure 3: The flowchart of BP algorithm based on WOA.

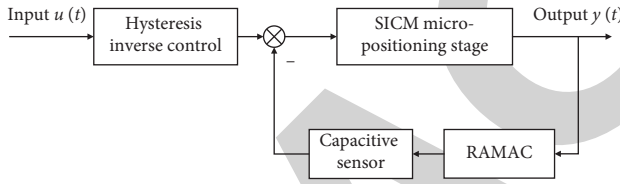

Figure 4: Control system of FRAMAC.

Among other control methods, for example, minimum-variance controls design the output of the closed-loop system as a moving average of order $d_0 - 1$. In the moving average control method, the output of the closed-loop system is designed to be of higher order, that is, the $d - 1$ closed-loop poles are designed at the origin, among which $d \geq d_0$.

The polynomial B can be decomposed into $B(q) = B^+(q)B^-(q)$, where B^+ represents a well damped zero, and in order to get the unique factorization form, we assume that B^+ is monic, where $R = R_1 B^+$. Solve R and S from the following equation:

$$q^{d-1}B^+\left(q^{-1}\right)C\left(q^{-1}\right) = A\left(q^{-1}\right)R\left(q^{-1}\right) + B\left(q^{-1}\right)S\left(q^{-1}\right). \tag{20}$$

Then, the control law of moving average is as follows:

$$u(k) = -\frac{S\left(q^{-1}\right)}{R\left(q^{-1}\right)}y(k). \tag{21}$$

It can be seen from this

$$A\left(q^{-1}\right)y(k) = B\left(q^{-1}\right)\left(-\frac{S\left(q^{-1}\right)}{R\left(q^{-1}\right)}\right)y(k) + C\left(q^{-1}\right)\xi(k). \tag{22}$$

Among them, $\deg R_1 = d - 1$ and $d = \deg A - \deg B^+$. When $B^+ = 1$ and $d = \deg A = n$, there is no zero cancellation. In this paper, the robust adaptive moving average control of piezoelectric ceramics will also adopt this simplest form.

2.2.2. Robust Control. In the actual system, there are always external disturbances. When the adaptive moving average control method is adopted, the system is difficult to return to the original equilibrium state. For this reason, this paper adopts Youla parameterization to improve the robustness of the controller.

When we solve the Diophantine equation, we usually get infinite solutions. If the order of the controller is certain, the solution is unique. This paper makes use of the characteristic of the Diophantine equation, and the robustness of adaptive moving average control is improved by adding one degree of freedom. The main idea of this is to set small gain at the frequencies in which the process is uncertain. For example, it is useful to set zero gain at the Nyquist frequency, that is, $S(-1) = 0$. It can be also required that the gain be zero at frequency ω_0. It means that

$$q^2 - 2\cos(\omega_0 h)q + 1 \tag{23}$$

is a factor of $S(q)$. In order to satisfy this condition, the order of the closed-loop system must be increased. The additional poles introduced are contained in the polynomial X. We want to improve its robustness by setting zero gain at the Nyquist frequency and requiring that $S(-1) = 0$. To do this, we introduce one more closed-loop pole which makes $X(q)$ stable. We choose

$$X(q) = q - x_0, \quad |x_0| < 1. \tag{24}$$

Polynomials Y can be arbitrarily chosen, and it can be of first order, $Y(q) = q - y_0$. On the basis of Youla Parameterization, it gives

$$S(q) = (q - x_0)S^0(q) - (q - y_0)A(q). \tag{25}$$

Because of $S(-1) = 0$, it gives

$$y_0 = -1 + \frac{(1 + x_0)S^0(-1)}{A(-1)}. \tag{26}$$

The robust controller is then characterized by

$$\begin{aligned} R(q) &= (q - x_0)R^0(q) + (q - y_0)B(q), \\ S(q) &= (q - x_0)S^0(q) + (q - y_0)A(q). \end{aligned} \tag{27}$$

The robust adaptive moving average control is obtained as follows:

$$u(k) = -\frac{S\left(q^{-1}\right)}{R\left(q^{-1}\right)}y(k), \tag{28}$$

where $\deg C = \deg A = 2$, $\deg B = 1$, $d_0 = \deg A - \deg B = 1$, and $B^+ = 1$.

2.2.3. FRAMAC. Based on the above introduction, the steps of the FRAMAC algorithm are as follows:

Step 1: the initial values $\widehat{\theta}(0)$, $P(0)$, and x_0, y_0 are calculated by formula (26)

Step 2: collect input voltage $y(k)$ and output displacement $u(k)$

Step 3: use WOA to establish the hysteretic polynomial inverse model of input voltage and output displacement

Step 4: take the output displacement $u(k)$ and input voltage $\widehat{y}(k)$ of the hysteresis polynomial as the input of the BP neural network, and take the input voltage $y(k)$ as the output to establish the hysteresis inverse model of the BP neural network based on WOA

Step 5: calculate the estimated value $\widehat{\theta}(k)$ by recursive least square method with forgetting factor

Step 6: equation (22) gives the R^0 and S^0

Step 7: equation (27) gives the R and S

Step 8: calculate the FRAMAC control $u(k)$ according to formula (28)

Step 9: $k \longrightarrow k + 1$, return to Step 2 for cyclic calculation

2.3. Experimental Facility. In order to verify the effectiveness of the FRAMAC Algorithm, the algorithm is verified on the piezoelectric ceramic micromotion platform and compared with the feedforward control algorithm, PID control algorithm, and feedforward PID feedback algorithm.

Figure 5 shows the physical diagram of the control system of the piezoelectric ceramic micropositioning stage. The experiment adopts P-621.ZCD produced by Germany Physik Instrumente Company (PI) with an open-loop resolution of 0.2 nm and a maximum displacement of 130 μm. The piezoelectric controller uses E-727.3CD Digital Multi-Channel Piezo Controller produced by PI Company to provide displacement drive for piezoelectric ceramics, and open-loop mode is used, and the input voltage range is −20 V~+120 V. The displacement sensor is D-E20.100 single-electrode capacitance position sensor made by PI Company. The dynamic resolution is less than 0.002%, and the static resolution is less than 0.001%. In this paper, the displacement sensor is used in the double range model and the measuring range is 200 μm. The data acquisition card is NIUSB-6210 produced by National Instruments Company, and the whole control system is controlled by LabVIEW programming.

3. Experimental Verification

3.1. Hysteresis Data Acquisition. In this paper, a triangular waveform voltage value of 0-80-0V is applied. The input voltage frequency is 0.5 Hz, and the displacement is collected every 0.1 s to obtain 1000 sets of data. Input voltage and output displacement are shown in Figure 6. Then, the hysteresis curve of piezoelectric ceramics is shown in Figure 7.

From Figure 7, we can see the multifunction relationship of the input and the output, that is, the same input corresponds to different outputs, and the same output corresponds to different inputs. Among them, the width of the hysteresis loop, that is, the maximum difference of the displacement between the rising curve and the descending curve, is 14.109, and the hysteresis value is 17.64%. This is due to the fact that piezoelectric ceramics as solids of ferroelectric materials possess the commonness of ferroelectric materials, that is, hysteresis nonlinearity [22].

3.2. The Modeling Results. In order to compare with other algorithms, the population size of the WOA is set as 30, and the final iteration number is set as 30. The input layer, hidden layer, and output layer of the BP neural network are 1, 1600 of 1000 ascending data and 1000 descending data are randomly selected as training data, and the other 400 data are model test data. The number of iterations is 100, the learning rate is 0.1, and the target rate is 0.00001. Because the test data are randomly selected, the average of the fitting error of 20 times is taken as the fitting error of backpropagation algorithm based on whale optimization algorithm. The identification results are shown in Figure 8, and the error sum of squares and the maximum displacement error of the hysteresis model are shown as follows:

$$\begin{aligned} J &= 0.3991, \\ e^* &= 0.2050. \end{aligned} \tag{29}$$

The BP neural network algorithm based on WOA shows the optimal identification effect in both the error sum of squares and the maximum error, the error sum of squares is 0.3991, and the maximum error is 0.2050 μm, which is 42.69%–77.42% lower than the common algorithm.

3.3. Verification of Control Algorithm. Feedforward control, PID feedback control, feedforward composite PID algorithm control, and FRAMAC algorithm are, respectively, used to control the system, the result of the FRAMAC algorithm is shown in Figure 9, and the control results are compared in Table 1.

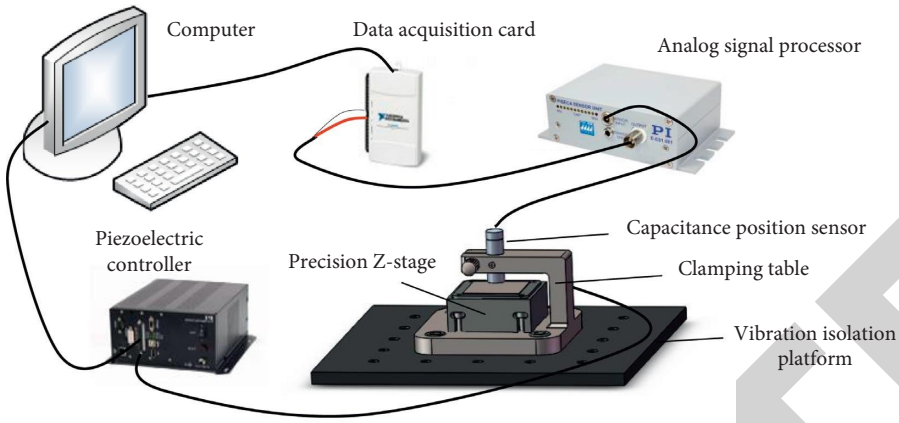

Figure 5: The control system of piezoelectric microposition platform.

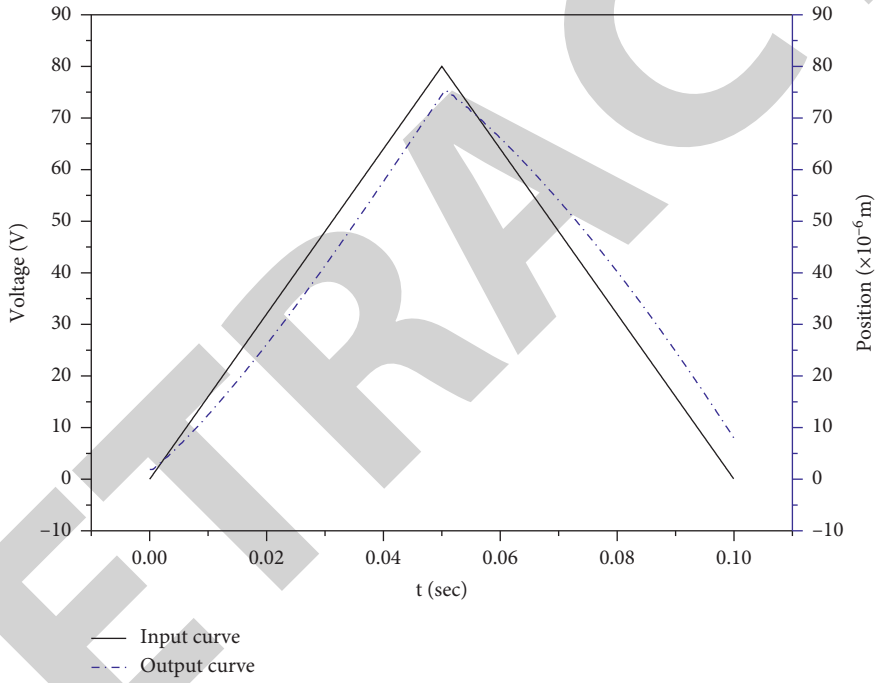

Figure 6: Triangle input voltage curve and output displacement curve.

It can be seen from Table 1 that the positioning error of the microplatform is the largest when only feedforward control is adopted because feedforward can only approximately linearize the hysteresis characteristic, unable to realize the requirement of steady state. Due to the disadvantages of PID feedback control, such as slow response speed, large overshooting, and poor anti-interference ability, it will produce certain positioning error. The feedforward composite PID feedback control method greatly reduces the positioning error and realizes the steady-state control of the linearized system. The error of the combined feedforward and feedback control method is much less than that of the single feedforward or feedback control method, which can achieve the goal of stable control when the system parameter changes and external disturbance acts on the system. At this time, the maximum difference of displacement between the ascending curve and the descending curve is 2.004 μm, only 2.51%.

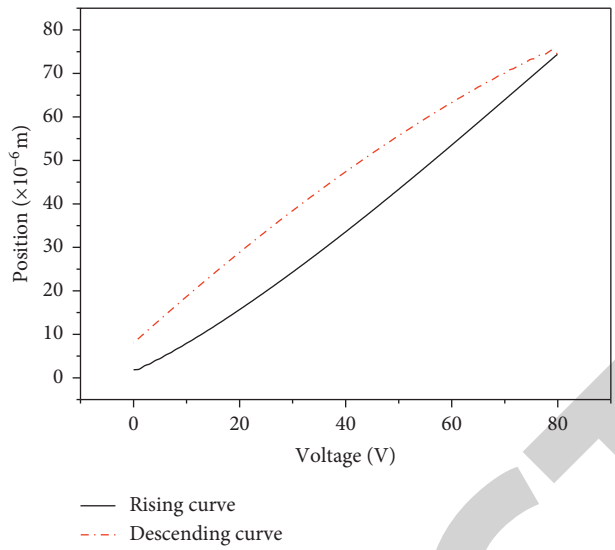

Figure 7: Hysteresis curve of piezoelectric ceramics.

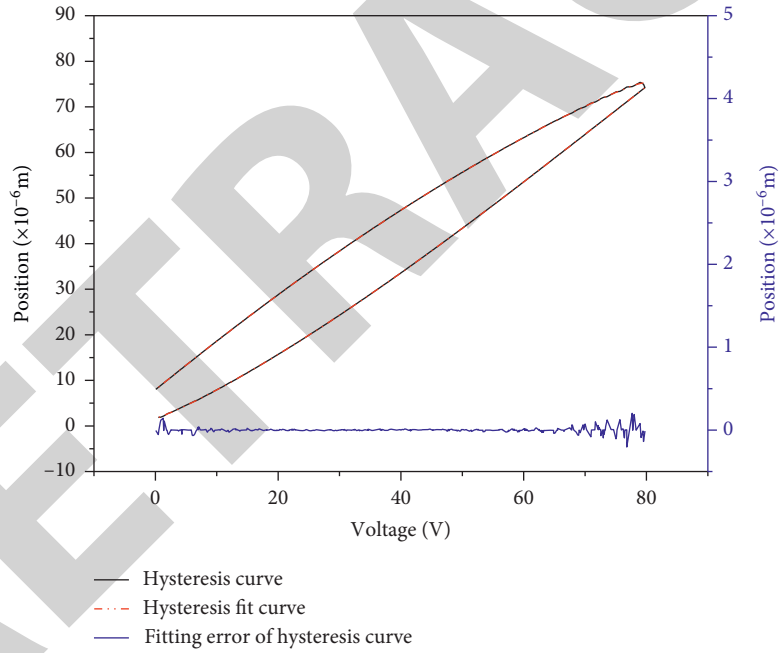

Figure 8: Modeling results of the BP algorithm based on WOA.

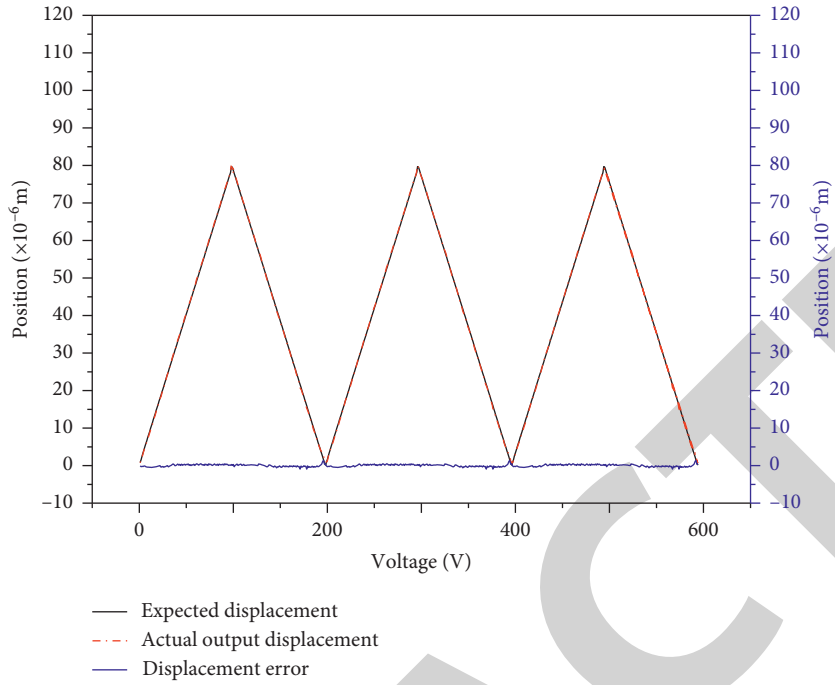

Figure 9: Results of FRAMAC.

Table 1: Comparison of different control algorithms.

Control algorithm	Feedforward	PID	Feedforward composite PID	FRAMAC
Error sum of squares	181.2620	59.3407	23.9626	19.9973

Therefore, in practical application, SICM microplatform scanning with this method has obtained higher probe positioning accuracy.

4. Conclusion

The positioning accuracy of the probe will directly affect the accuracy of the sample scanning. Based on the hysteresis model of the micromotion platform, this paper conducts an in-depth study on the control method. According to back-propagation algorithm based on whale optimization algorithm, the traditional analytical method is abandoned to calculate the hysteresis inverse model. The output displacement of the piezoelectric ceramic controller is taken as the input, and the input voltage is taken as the output. The hysteresis inverse model is directly established as the feedforward of the system. The moving average control method is improved by adaptive technology and robust technology, and the influence of "uncertainty" and external disturbance on the positioning accuracy of piezoelectric ceramics is effectively reduced. The FRAMAC algorithm is formed, and the effect of hysteresis characteristics on the piezoelectric ceramic control is effectively reduced. The maximum displacement difference between the rising curve and the falling curve is 2.004 μm, and the hysteresis decreases by 15.13% to 2.51%. Through experimental verification, the error of the FRAMAC method is far less than that of the widely used PID, which solves the shortcoming of large positioning error of the piezoceramics control probe, improves the positioning accuracy of the probe in the experimental process, and creates conditions for the high-precision scanning of samples.

Data Availability

The data used to support the findings of this study are available from the corresponding author upon request.

Conflicts of Interest

The authors declare that they have no conflicts of interest.

Acknowledgments

This work was supported by Grant 2014GZ0131 (Sichuan Science and Technology Research Project).

References

[1] P. K. Hansma, B. Drake, O. Marti et al., "The scanning ion-conductance microscope," *Science*, vol. 243, no. 4891, pp. 640–643, 1989.

[2] L. A. Bottomley, J. E. Coury, and P. N. First, "Scanning probe microscopy," *Analytical Chemistry*, vol. 70, no. 12, pp. 425–476, 1998.

[3] F. M. Madder, D. Perry, R. Brooks et al., "Nanoscale surface charge visualization of human hair," *Analytical Chemistry*, vol. 91, pp. 4632–4639, 2019.

[4] M. Pellegrino, P. Orsini, M. Pellegrini et al., "Weak hydrostatic forces in far-scanning ion conductance microscopy used to guide neuronal growth cones," *Neuroscience Research*, vol. 69, no. 3, pp. 234–240, 2011.

[5] Y. E. Korchev, J. Gorelik, M. J. Lab et al., "Cell volume measurement using scanning ion conductance microscopy," *Biophysical Journal*, vol. 78, no. 1, pp. 451–457, 2000.

[6] M. Pellegrino, P. Orsini, M. Pellegrini et al., "Measuring the elastic properties of living cells through the analysis of current-displacement curves in scanning ion conductance microscopy," *Pfluegers Archiv: European Journal of Physiology*, vol. 463, 2012.

[7] C. Zhu, W. Shi, D. L. Daleke, and L. A. Baker, "Monitoring dynamic spiculation in red blood cells with scanning ion conductance microscopy," *The Analyst*, vol. 143, no. 5, pp. 1087–1093, 2018.

[8] Y. Ting and T. Van, "Design and performance evaluation of an exponentially weighted moving average-based adaptive control for piezo-driven motion platform," *Advances in Mechanical Engineering*, vol. 10, no. 6, pp. 1–14, 2018.

[9] L. Yuan, F. Qian, and S. Xu, "Control method for piezoelectric actuator based on single neuron PID controller," *Computer Measurement & Control*, vol. 23, no. 11, pp. 3657–3660, 2015.

[10] S. Xu, "New high speed current controlled amplifier for pzt multilayer stack actuators," in *Proceedings of the 8th International Conference on New Actuator*, Bremen, Germany, June 2002.

[11] K. Furutani, M. Urushibata, and N. Mohri, "Improvement of control method for piezoelectric actuator by combining induced charge feedback with inverse transfer function compensation," in *Proceedings of the IEEE International Conference on Robotics and Automation*, Washington, DC, USA, April 2002.

[12] X. Wang and G. Jiang, "Hysteresis modeling and control simulation of piezoeletric ceramic," *Piezoelectrics & Acoustooptics*, vol. 37, no. 6, pp. 926–929, 2015.

[13] K. Kuhnen and H. Janocha, "Adaptive inverse control of piezoelectric actuators with hysteresis operators," in *Proceedings of the 1999 European Control Conference (ECC)*, Karlsruhe, Germany, October 1999.

[14] J. A. Mynderse and G. T.-C. Chiu, "Two-Degree-of-freedom hysteresis compensation for a dynamic mirror actuator," *IEEE/ASME Transactions on Mechatronics*, vol. 21, no. 1, pp. 29–37, 2016.

[15] Z. Yu, Y. Wang, K. Cao et al., "Hysteresis compensation and composite for piezoelectric actuator," *Optics and Precision Engineering*, vol. 25, no. 8, pp. 2113–2120, 2017.

[16] S. Mirjalili and A. Lewis, "The whale optimization algorithm," *Advances in Engineering Software*, vol. 95, pp. 51–67, 2016.

[17] R. Kumar and V. K. Sharma, "Whale optimization controller for load frequency control of a two-area multi-source deregulated power system," *International Journal of Fuzzy Systems*, vol. 22, no. 1, pp. 122–137, 2020.

[18] M. A. E. Aziz, A. A. Ewees, and A. E. Hassanien, "Whale optimization algorithm and moth-flame optimization for multilevel thresholding image segmentation," *Expert Systems with Applications*, vol. 83, pp. 242–256, 2017.

[19] Y. Yu, C. Zhang, and M. Zhou, "Narmax model-based hysteresis modeling of magnetic shape memory alloy actuators," *IEEE Transactions on Nanotechnology*, vol. 19, pp. 1–3, 2019.

[20] J. Yang, M. Xi, B. Jiang et al., "Robust 6-DoF estimation for IIoT based on multi-branch network," *IEEE Transactions on Industrial Informatics*, vol. 17, no. 4, pp. 2767–2775, 2020.

[21] J. Liu and K. Zhou, "Neural networks based modeling and robust control of hysteresis," in *Proceedings of the 2016 35th chinese control conference (CCC)*, Chengdu, China, July 2016.

[22] Q. Xu, "Identification and compensation of piezoelectric hysteresis without modeling hysteresis inverse," *IEEE Transactions on Industrial Electronics*, vol. 60, no. 9, pp. 3927–3937, 2013.